applied sciences

MDPI

Article

The Synthesis of Ag/TiO_2 via the DC Magnetron Sputtering Method and Its Application in the Photocatalytic Degradation of Methyl Orange in Na_2SO_4 Solution

Li Sun [1], Zhuoqun Que [1], Ting Ruan [1], Zhigang Yuan [1,*], Wenbang Gong [1], Shunqi Mei [1], Zhen Chen [1] and Ying Liu [2]

[1] Hubei Key Laboratory of Digital Textile Equipment, Wuhan Textile University, Wuhan 430073, China; sunli@wtu.edu.cn (L.S.); 2115053018@mail.wtu.edu.cn (Z.Q.); ruanting97@126.com (T.R.); 2007027@wtu.edu.cn (W.G.); sqmei@wtu.edu.cn (S.M.); 2015035@wtu.edu.cn (Z.C.)

[2] Test Center, Wuhan Textile University, Wuhan 430073, China; 2015060@wtu.edu.cn

* Correspondence: yuanzhigang@wtu.edu.cn; Tel./Fax: +86-027-5936-3391

Abstract: TiO_2 and TiO_2 films modified with Ag (Ag/TiO_2) were prepared via the DC magnetron sputtering method and the degree of modification was controlled via the sputtering power and time of Ag. The microstructures and properties of these films were characterized using field emission scanning electron microscopy, X-ray diffractometry, ultraviolet–visible diffuse reflectance spectrometry, atomic force microscopy, and X-ray photoelectron spectroscopy (XPS). The results show that the prepared films have an anatase structure. Compared with pure TiO_2, Ag deposition can improve the utilization of light. The three-dimensional images of Ag/TiO_2 clearly show that with the increase in Ag sputtering power and sputtering time, Ag particles on the surface of the film gradually increase, and the structure of the film is relatively dense. The photocatalytic effect of Ag/TiO_2 films is the best when the Ag sputtering power is 5 W and the sputtering time is 50 s. Under high-pressure mercury lamp irradiation, the photocatalytic degradation rate of methyl orange (MO) in pure MO solution with Ag/TiO_2-5 W-50 s can reach 100% within 55 min, whereas that in MO-Na_2SO_4 mixed solution can reach 99.55% within 65 min. The results suggest that the presence of Na_2SO_4 in MO solution can inhibit the degradation of MO using Ag/TiO_2, the result of XPS suggests that Na_2SO_4 accelerates the oxidation of Ag, which may lead to an increase in the recombination rate of photogenerated electron–hole pairs and a decrease in the degradation rate. During the process of recycling photocatalysts, the degradation rate of MO was apparently reduced. A possible reason is that the Ag particles have been oxidized and products of photocatalytic degradation are on the surface of the photocatalyst. The photocatalytic degradation mechanism was studied.

Keywords: photocatalytic property; magnetron sputtering; Ag-modified TiO_2; structural analysis

Citation: Sun, L.; Que, Z.; Ruan, T.; Yuan, Z.; Gong, W.; Mei, S.; Chen, Z.; Liu, Y. The Synthesis of Ag/TiO_2 via the DC Magnetron Sputtering Method and Its Application in the Photocatalytic Degradation of Methyl Orange in Na_2SO_4 Solution. *Appl. Sci.* **2024**, *14*, 4014. https://doi.org/10.3390/app14104014

Academic Editor: Alexander N. Pisarchik

Received: 13 April 2024
Revised: 1 May 2024
Accepted: 4 May 2024
Published: 9 May 2024

1. Introduction

In both industrial and agricultural settings, the discharge of dye wastewater often contains numerous hazardous organic pollutants. These organic pollutants exhibit strong toxicity and carcinogenicity, posing serious threats and impacts to both human health and the natural environment. For example, methyl orange (MO, $C_{14}H_{14}N_3NaO_3S$) is used as a dye in the textile industry, and in the process of printing and dyeing, sodium sulfate (Na_2SO_4) is often added as a dyeing and finishing auxiliary. After dyeing and finishing, great amounts of MO and Na_2SO_4 are discharged into the water, which will pollute the water and adversely affect the aquatic ecosystems. Since MO is difficult to biodegrade and can exist in water for a long time, azo dye wastewater is one of the wastewaters that needs to be treated urgently today. The addition of Na_2SO_4 undoubtedly further increases the complexity of the wastewater, so it is very necessary to study the effect of Na_2SO_4 on the water treatment [1,2]. In recent decades, techniques such as adsorption and photocatalytic

degradation have been widely applied [3]. Photocatalytic degradation typically results in the formation of smaller, harmless molecules or ions such as water, carbon dioxide, oxygen, and non-toxic organic acids. These degradation products are usually less toxic and more easily broken down via natural processes or further processed, thus reducing their impact on the environment and human health. As a result, there is increasing attention on methods for degrading organic compounds in water.

TiO_2 is considered an ideal semiconductor photocatalyst material due to its high catalytic activity, non-toxicity to the human body, and strong oxidizing and reducing properties [4]. At present, metal doping [5,6] has been discovered to adjust the energy band gap of TiO_2 to different degrees, non-metal doping [7], metal deposition [8], and other methods to broaden the light response range of TiO_2 film. When a certain number of metal ions are doped into TiO_2, electron trapping centers are formed, which promote the migration of electrons. At the same time, it may change the crystallinity of TiO_2, produce some surface defects, slow down the recombination of electron–hole pairs, and make TiO_2 generate more active free radicals to improve photocatalytic activity [9]. Noble metal deposition [10–12] is a method that is used to improve its own catalytic activity by depositing noble metals on the surface of nano-TiO_2. Due to the large Fermi level difference between nano-TiO_2 and noble metals, the Fermi level can be reduced via noble metal deposition [13,14]. The surface electrons of TiO_2 with high energy level are transferred to the noble metal until the Fermi levels are the same, and the electron distribution of TiO_2 changes to obtain photogenerated electrons, reduce the recombination rate of photogenic charge carrier, and improve the catalytic efficiency of the photocatalyst [15–17]. However, the above research mainly focuses on the photocatalytic degradation of wastewater systems containing only dyes. The actual dye wastewater system is complex, containing salts and other additives. The research on the photocatalytic degradation of complex wastewater systems is not sufficient. In addition, the use of small photocatalyst powders in water-based systems (often contaminated slurries) can lead to problems with powder handling and the collection of the photocatalysts used [18]; improper handling can cause secondary pollution. The photocatalyst is easy to recover and reuse, which is beneficial for reducing costs. The practical method to solve these issues is to fix TiO_2 on a stable substrate.

In this paper, TiO_2 and TiO_2 modified with Ag (Ag/TiO_2) were prepared via DC magnetron sputtering on glass. The influence of different contents of Ag modification on photocatalytic performance was studied. Using FESEM, XRD, UV-VIS DRS, AFM, and XPS, the microstructures and properties of these films were characterized. Methyl orange (MO) solution and the mixed solution of MO and sodium sulfate (Na_2SO_4) were used as simulated wastewater. The photocatalytic properties of photocatalysts and the effect of Na_2SO_4 on the photocatalytic degradation of dyes are discussed. The recycling ability of photocatalysts deposited on glass and the mechanism of the photocatalytic degradation of dye were investigated through cyclic experiments.

2. Materials and Methods

Ti target (99.99%) and Ag target (99.99%) were used as sputtering targets. Ag/TiO_2 films were prepared on glass slides, monocrystalline silicon, and quartz glass substrates via the DC magnetron sputtering method [12,17]. Firstly, the substrate was placed in anhydrous ethanol and washed twice with an ultrasonic cleaner for 15 min each; then, the washed substrate was placed in ultrapure water and washed twice with an ultrasonic cleaner for 15 min each. Secondly, the targets were mounted on the corresponding bases, respectively, and the substrate was fixed on the sample fixing table. The targets were located below the sample and sputtered upwards at an angle of 60°, and the distance between the targets and the substrate was about 100 mm. The sputtering process for preparing TiO_2 films is as follows: Before sputtering, the deposition chamber was evacuated to 1×10^{-3} Pa, and then Ar (99.999%) and O_2 (99.999%) were introduced into the vacuum chamber. The gas flow rates of Ar and O_2 were 12 sccm and 4 sccm, respectively. During the deposition process, the total sputtering pressure of the Ti target and the substrate temperature were maintained

at 0.7 Pa and 300 °C, respectively. The total deposition time and the sputtering power of the Ti target were 7200 s and 120 W, respectively. The preparation process of the Ag-modified TiO_2 (Ag/TiO_2) films is as follows: First, the TiO_2 films were deposited using the Ti target at a total pressure of 0.7 Pa. Next, the Ti target was turned off, the O_2 was stopped, and the Ar flow rate remained unchanged. Then, the Ag target was turned on. The modification of TiO_2 film surfaces with different amounts of Ag was performed by controlling the sputtering power and time of Ag. In maintaining a constant sputtering power of 5 W for Ag targets, the corresponding sputtering time was 50 s (Ag/TiO_2-5 W-50 s), 100 s (Ag/TiO_2-5 W-100 s), and 150 s (Ag/TiO_2-5 W-150 s), respectively. When the sputtering power of the Ag target was 10 W and 15 W, the corresponding sputtering time was 100 s, respectively (Ag-TiO_2-10 W-100 s and Ag/TiO_2-15 W-100 s).

Then, the sputtered samples were annealed, and a tubular atmosphere furnace was used. The heating and cooling rate was 4 °C/min; the temperature increased from the initial temperature to 450 °C, was kept for 90 min, and the temperature then dropped from 450 °C to room temperature after 90 min.

Using a field emission scanning electron microscope (FESEM: JSM-7800, Tokyo, Japan) with an accelerating voltage of 15.0 kV, energy-dispersive spectroscopy (EDS) in field emission scanning electron microscopy, and X-ray photoelectron spectroscopy (XPS, Thermo SCIENTIFIC (Waltham, MA, USA) K-Alpha, JEOL with Mg Kα X-ray light source (photon radiation energy of 1486.68 eV)), the morphologies and structural and compositional properties of the TiO_2 and Ag/TiO_2 films were examined. X-ray diffraction (XRD, Empyrean Panaco Netherlands, Cu-Kα radiation) was used to describe the film's crystalline structure. The scan speed was 2.33 °/min, the step length was 0.06, and the 2θ scan range was 10° to 80°. The spectral range of the UV–VIS diffuse reflectance spectra (UV–VIS DRS) of all samples was 200–800 nm. It was measured with a UV–VIS–NIR spectrophotometer (UV-VIS–NIR: Shimadzu Solid Spece-3700 (Shimadzu, Beijing, China)). The Kubelka–Munk function was used to convert the UV-VIS DRS to the absorption coefficient F(R). Using the Tauc method, the energy band gap (E_g) of the samples was calculated from the plot of $(F(R)h\nu)^{1/2}$ against hν [19]. The surface topography of the films was analyzed using an atomic force microscope (AFM, Shimadzu SPM-9700) operated in the tapping mode with a measured area of 5 × 5 μm^2. The photocatalytic activity was studied under a mercury lamp with a power of 300 W. MO in pure solution or MO-Na_2SO_4 mixed solution was the object of photocatalytic degradation. UV-VIS spectrophotometry (UV-VIS: Beijing Puxi Tu-1950) was used to determine the concentration of MO solution both before and after the photocatalytic experiment, with the maximum absorption wavelength being 459 nm.

First, the prepared photocatalysts (4.5 cm × 2.5 cm) were placed in methyl orange (MO) solution (15 mL) at a concentration of 10 mg/L. The dye solution was then held under dark conditions until it reached absorption–desorption equilibrium. Then, the dye solution containing photocatalysts was irradiated at a position 10 cm below the high-pressure mercury lamp (300 W). In keeping the experimental conditions unchanged, the photocatalyst was used to degrade the MO solution (10 mg/L) containing Na_2SO_4 (12.5 g/L) (MO-Na_2SO_4 mixed solution). Four cycles of testing were conducted in order to characterize the cycling stability of the films' photocatalytic performance. After photocatalytic degradation, the photocatalyst was taken out of the solution and cleaned by rinsing it with ultrapure water. Then, the film was dried at room temperature and reused for the photocatalytic degradation of MO. The degradation rate can be calculated with the following formula [20]:

$$\eta\% = \frac{C_0 - C_t}{C_0} \times 100\% \quad (1)$$

where η is the degradation rate of MO in pure MO solution or MO-Na_2SO_4 mixed solution, C_0 (mg L^{-1}) is the initial concentration of the MO, and C_t (mg L^{-1}) is the concentration of the MO solution at time t (min).

3. Results

The XRD patterns of TiO_2 and Ag/TiO_2 films with different sputtering power and times of Ag are shown in Figure 1a. The diffraction peaks at 25.1°, 37.7°, 47.9°, 53.8°, 55.0°, and 62.5° correspond to the characteristic planes (101), (004), (200), (105), (211), and (204) planes of TiO_2 (JCPDS No. 21-1272), respectively [21,22]. The results demonstrate that TiO_2 film has an anatase structure. The diffraction peaks at 38.0° and 44.1° correspond to the (111) and (200) crystal planes of Ag (JCPDS Card 01-1164), respectively. When the sputtering time of Ag is 100 s, with the increase in the sputtering power of Ag, the diffraction peak intensity of TiO_2 decreases gradually; the diffraction peak intensity of Ag also increases gradually, which indicates that the Ag deposited on the surface of TiO_2 film increases gradually with the increase in the sputtering power of Ag, shown in Figure 1a. The XRD patterns of Ag/TiO_2 thin films with a sputtering power of 5 W and different sputtering times for Ag are shown in Figure 1b. The diffraction peaks appear at 25.1° corresponding to the (101) plane of anatase TiO_2, at 38.0° and 44.1° corresponding to (111) and (200) crystal planes of Ag, respectively. With the increased sputtering time of Ag, the diffraction peak intensity of TiO_2 decreases gradually and the diffraction peak intensity of Ag increases gradually, as shown in Figure 1b. When the sputtering power and the sputtering time of Ag are 5 W and 150 s, respectively, the diffraction peak of TiO_2 is very weak. The intensity of the diffraction peak of Ag/TiO_2-5 W-150 s at 38.0° and 44.1° is stronger than that of Ag/TiO_2-15 W-100 s. These results show that the Ag deposition on the TiO_2 surface increases rapidly with increasing sputtering time.

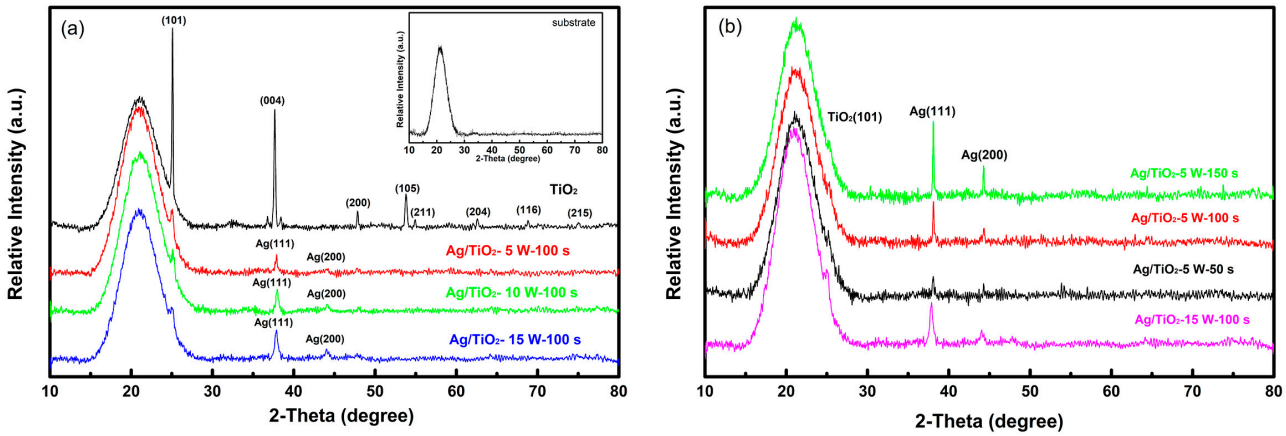

Figure 1. XRD patterns of films (**a**) TiO_2 and Ag/TiO_2 with different sputtering powers of Ag (**b**) Ag/TiO_2 with different sputtering times of Ag.

Figure 2 shows the surface morphologies of TiO_2 and Ag/TiO_2 films. It is possible to clearly observe the uniform small particles of TiO_2 deposited on the substrate in Figure 2a, which can make particles come into contact with the more suitable water and oxygen in the solution and produce more highly oxidized hydroxyl radicals; this leads to an increase in the photocatalytic activity of the catalysts [23]. When the sputtering power is 5 W, and the sputtering times are 50 s and 100 s, respectively, Ag particles are very small and evenly distributed on TiO_2 particles, as shown in Figure 2b,c. When the sputtering power is 5 W and the sputtering time is 150 s, it can be observed in Figure 2d that the distribution of Ag particles is uneven, and the magnitude of the Ag particles is much greater than that in Figure 2b and c. When the sputtering power is 10 W and the sputtering time is 100 s, the distribution of Ag particles is very uneven, as shown in Figure 2e. The distribution range of the Ag particle size is very wide and much wider than that shown in Figure 2d. The mass of Ag per unit area shown in Figure 2e is lower than that deposited at 5 W and 150 s as shown in Figure 2d. The results correspond to those of XRD in Figure 1. When the sputtering power is 15 W and the sputtering time is 100 s, the surface of the particles is smooth and somewhat round, and the Ag particles are shown to be uniformly and densely distributed

in Figure 2f. The experimental results indicate that sputtering power and time not only seriously affect the particle size but also affect the uniformity of particle distribution. By comparing samples with different sputtering powers and sputtering times, it can be found that Ag particles sputtered at 5 W and 50 s (Ag/TiO_2-5 W-50 s) are more uniform and smaller in size, which can reduce the recombination rate of photogenic electron–hole pairs and enhance the catalytic productivity of the photocatalyst [15,16]. Figure 2g shows the cross-section morphologies of TiO_2. The thickness of the film is about 235 nm. It was calculated that the Ag particle sizes of Ag/TiO_2-5 W-50 s, Ag/TiO_2-5 W-100 s, Ag/TiO_2-5 W-150 s, Ag/TiO_2-10W-100 s, and Ag/TiO_2-15 W-100 s are 44 nm, 99 nm, 65 nm, 108 nm, and 92 nm, respectively. The results suggest that the Ag particles sputtered at 5 W and 50 s favored the photocatalytic degradation of MO. This is because small isolation facilitates the separation of photogenic charge carriers [24].

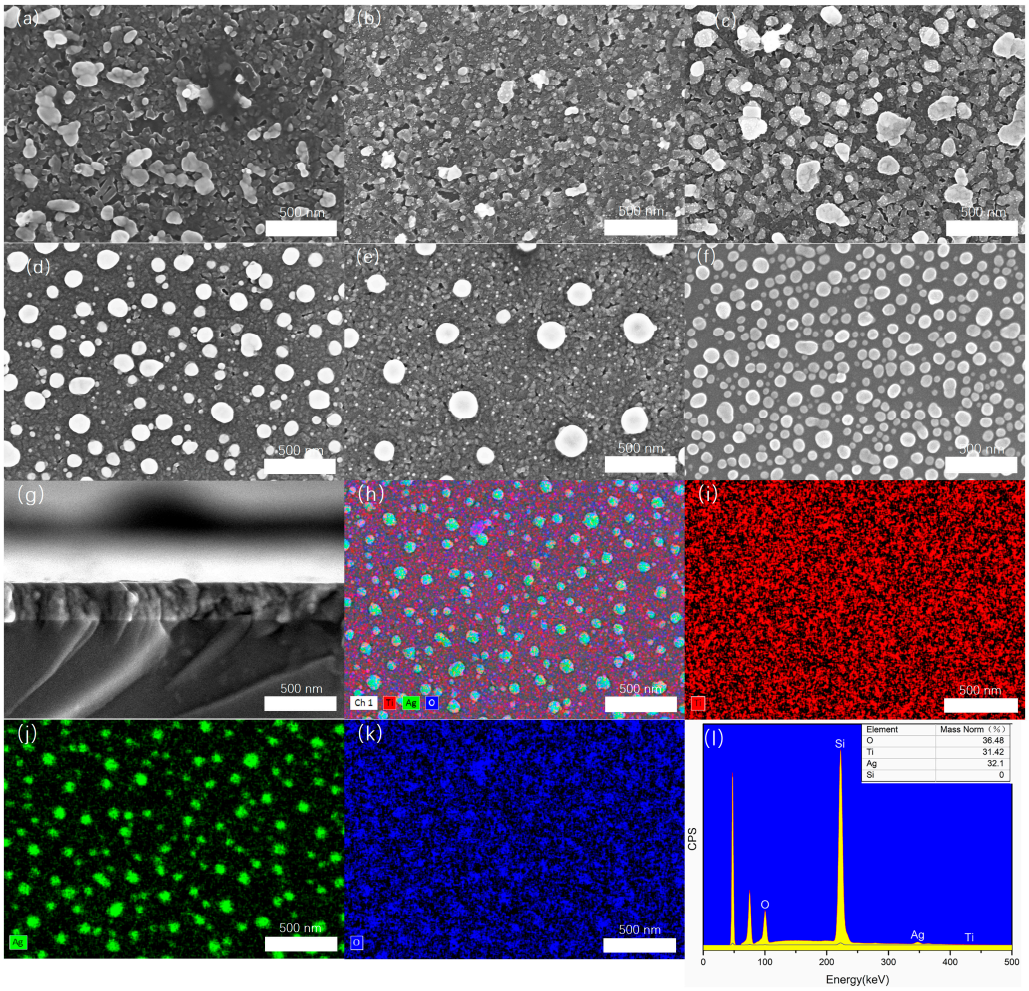

Figure 2. SEM images and mapping of elemental analyses of TiO_2 (**a**), Ag/TiO_2 (**b**), Ag/TiO_2-5 W-50 s, (**c**) Ag/TiO_2-5 W-100 s, (**d**) Ag/TiO_2-5 W-150 s, (**e**) Ag/TiO_2-10 W-100 s, and (**f**) Ag/TiO_2-15 W-100 s; (**g**) cross-section of TiO_2; (**h**–**k**) EDS mappings of Ag/TiO_2-5 W-150 s; and (**l**) EDS point analysis of Ag/TiO_2-5 W-150 s films.

To obtain high-quality signals of chemical compositions, the sample of Ag/TiO_2-5 W-150 s was measured using EDS, as shown in Figure 2h–k. The EDS analysis was performed to confirm the presence of different elements in the composite. It is possible to observe that the material contains three elements, Ti, Ag, and O, which are uniformly distributed in Figure 2h–k. The EDS point analysis is shown in Figure 2l; Ti, Ag, and O are detected. Other elements may come from pollution and substrates.

The 3D surface topographies and roughness of films are studied via AFM in Figure 3 and Table 1. It is seen that the 3D surface topographies of all samples are columnar structures. Figure 3a shows the 3D surface topography of TiO_2; it can be seen that the TiO_2 nanoparticles are uniformly dispersed on the entire substrate surface. When Ag with a power of 5 W and a sputtering time of 50 s is used for the surface modification of TiO_2, the average diameter of the columnar structure is the smallest in Figure 3b. The maximum constructive height is 102.26 nm corresponding to the Ag/TiO_2-5 W-100 s film in Figure 3c. With the increase in the sputtering time of Ag, the constitutive height of the Ag/TiO_2-5 W-50 s film as shown in Figure 3b first increases from 41.27 nm to 102.26 nm of Ag/TiO_2-5 W-100 s film, shown in Figure 3c, and then decreases to 80.42 nm of the Ag/TiO_2-5 W-150 s film, shown in Figure 3d. With the increase in the sputtering power of Ag, the constitutive height of Ag/TiO_2-10 W-100 s film shown in Figure 3e first decreases to 63.29 nm from 102.26 nm of Ag/TiO_2-5 W-100 s, shown in Figure 3c, and then increases to 70.92 nm of Ag/TiO_2-15 W-100 s film, as shown in Figure 3f.

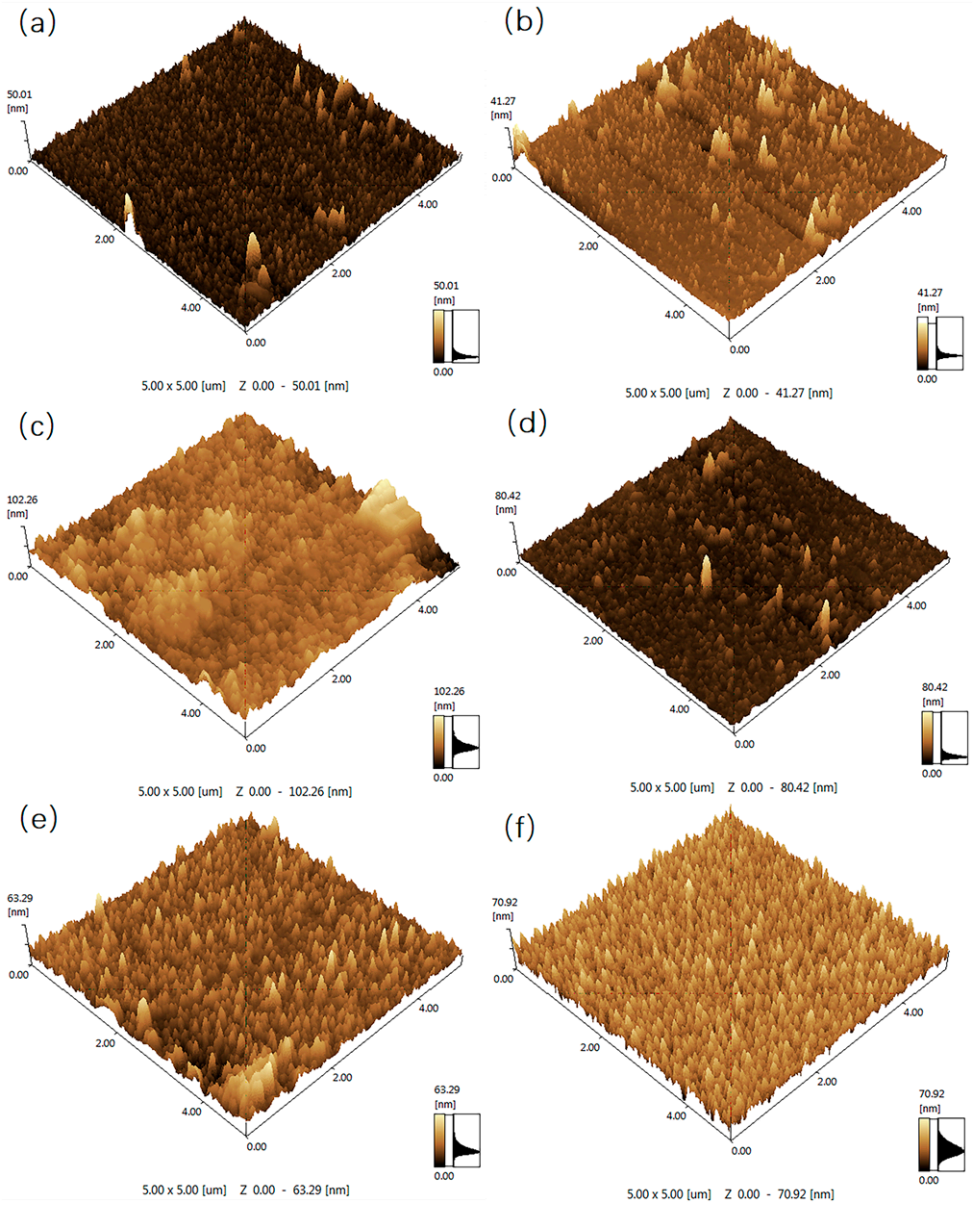

Figure 3. A set of 3D diagrams of the following films: (**a**) TiO_2, (**b**) Ag/TiO_2-5 W-50 s, (**c**) Ag/TiO_2-5 W-100 s, (**d**)Ag/TiO_2-5 W-150 s, (**e**) Ag/TiO_2-10 W-100 s, and (**f**) Ag/TiO_2-15 W-100 s.

Table 1. Surface roughness of TiO_2 and Ag/TiO_2.

Sample	Ra (nm)
TiO_2	2.025
Ag/TiO_2-5 W-50 s	2.203
Ag/TiO_2-5 W-100 s	7.534
Ag/TiO_2-5 W-150 s	3.118
Ag/TiO_2-10 W-100 s	4.723
Ag/TiO_2-15 W-100 s	7.082

The surface roughness is shown in Table 1. The maximum surface roughness is 7.534 nm, corresponding to the Ag/TiO_2-5 W-100 s film detailed in Table 1. With the increase in the sputtering time of Ag, the surface roughness of the film increases from 2.203 nm to 7.534 nm and then decreases from 7.534 nm to 3.118 nm. With the increase in the sputtering power of Ag, the surface roughness of the film decreases from 7.534 nm to 4.723 nm and then increases from 4.723 nm to 7.082 nm. The results indicate that the sputtering power and time of Ag have an impact on the surface roughness of the film.

Figure 4a–c show the UV–Vis DRS of the samples. Compared with the UV–Vis DRS of TiO_2 in Figure 4a, the UV–Vis DRS of Ag/TiO_2 exhibits a redshift in Figure 4b. It can be discovered that when the deposition time of Ag is 100 s, the larger the deposition power of Ag, the greater the redshift of the absorption edge, and the degree of redshift increases with the increases in the sputtering power of Ag, as shown in Figure 4b. And, in Figure 4c, it is shown that when the deposition power of Ag is 5 W, as the deposition time of Ag is prolonged, the absorption edge first blueshifted and then redshifted. Compared with TiO_2, Ag/TiO_2 films show different degrees of redshift. The findings revealed that the surface modification of small Ag particles has a considerable impact on optical properties. The reason for this phenomenon may be that the decrease in the particle size leads to the increase in the internal stress P ($P = 2\gamma/r$, where γ is the surface energy and r is the particle radius), and the overlap of electron wave functions results in a redshift in the absorption limit [20]. The absorption displays the localized surface plasmon resonance of Ag nanoparticles centered at around 520 nm for the Ag/TiO_2 films [25]. The band gaps (E_g) of Ag/TiO_2 and TiO_2 are determined through the Tauc graphical method to analyze the optical characteristics of the films, as shown in Figure 4d–f using Equation (2) [26]:

$$\alpha h\nu = C\left(h\nu - E_g\right)^{1/2} \quad (2)$$

where α is the absorption coefficient, C is constant, h is the photon energy, and E_g is the band gap. The E_g of the samples are estimated from the Tauc plots, via the extrapolation of the linear part of the Tauc plot at zero F(R) [27,28], as shown in Figure 4d–f. The E_g of pure TiO_2 is 3.28 eV in Figure 4d. The E_g of Ag/TiO_2-5 W-100 s, Ag/TiO_2-10 W-100 s, and Ag/TiO_2-15 W-100 s are 2.43 eV, 2.5 eV, and 2.64 eV in Figure 4e, respectively. The E_g of Ag/TiO_2-5 W-50 s, Ag/TiO_2-5 W-100 s, and Ag/TiO_2-5 W-150 s are 2.66 eV, 2.7 eV, and 2.59 eV in Figure 4f, respectively. When the Ag deposition power is 5 W and the deposition time is 100 s, the corresponding band gap of 2.43 eV is the minimum. These results indicate that Ag modification can change the band gap of TiO_2. Compared with pure TiO_2, if the amount of silver modification is appropriate, the photocatalyst can expand its light response range and produce a certain redshift.

The luminous group of MO is a nitrogen-conjugated double bond. In the experiment, the value of the characteristic peak decreased over time, indicating that the concentration of MO gradually decreased. After the photocatalytic reaction reached equilibrium, the recycled photocatalyst was immersed in water and no dye color was found. This indicates that the degradation reaction is mainly photocatalytic degradation, and the dye molecules are degraded through photocatalysis rather than adsorption.

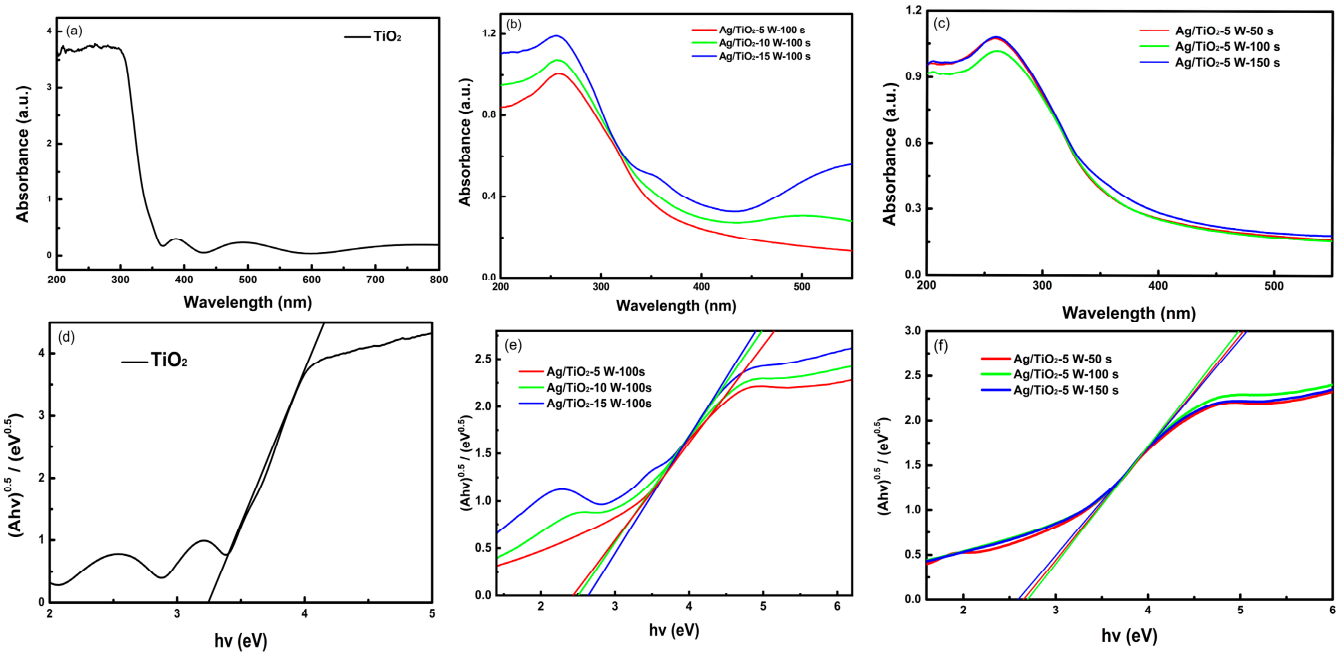

Figure 4. UV-Vis DRS of (**a**) TiO_2, (**b**) Ag/TiO_2-5 W-100 s, Ag/TiO_2-10 W-100 s, and Ag/TiO_2-15 W-100 s photocatalysts; (**c**) Ag/TiO_2-5 W-50 s, Ag/TiO_2-5 W-100 s, and Ag/TiO_2-5 W-150 s photocatalysts; Tauc plots obtained for (**d**) TiO_2 photocatalysts, (**e**) Ag/TiO2-$_5$ W-100 s, Ag/TiO_2-10 W-100 s, and Ag/TiO_2-15 W-100 s photocatalysts; and (**f**) Ag/TiO_2-5 W-50 s, Ag/TiO_2-5 W-100 s, and Ag/TiO_2-5 W-150 s photocatalysts.

The photocatalytic activity of Ag/TiO_2 and TiO_2 was investigated by measuring the UV-Vis spectra of MO solution after the photocatalytic degradation reaction under the same conditions. Figure 5a shows the UV-Vis absorption spectra of MO before (Co) and after photocatalytic degradation through Ag/TiO_2 and TiO_2 in pure MO solution. The results suggest that the photocatalytic effect is the best when the sputtering power is 5 W and the sputtering time of Ag is 50 s. Figure 5b shows UV-Vis absorption spectra of MO solution with an initial concentration of 10 mg L^{-1} under different illumination times during the photocatalytic degradation of MO using Ag/TiO_2-5 W-50 s in pure MO solution. Figure 5c shows the degradation rate of MO solution via Ag/TiO_2 modified using Ag with different sputtering power and sputtering times of Ag in pure MO solution. It demonstrates that the degradation rate of MO solution using Ag/TiO_2-5 W-50 s can reach 100% within 55 min. The results also indicate that although the redshift of Ag/TiO_2-5 W-50 s is not as significant as that of Ag/TiO_2 using the high-power and long-time sputtering of Ag, small particles of Ag can help to improve the separation of photogenerated electron–hole pairs, thereby enhancing the degradation effect. The main reason for this phenomenon may be (1) the interface between Ag nanoparticles deposited on the TiO_2 surface and TiO_2 nanoparticles, forming a Schottky barrier that enables the continuous migration and enrichment of photogenerated electrons to Ag particles, and facilitates the separation of electrons and holes, thus improving the photocatalytic activity [29,30]; (2) the Ag nanoparticles on the TiO_2 surface, causing the electron cloud density on the TiO_2 surface to decrease, which facilitates the adsorption of O_2 on the (101) crystal surface of anatase TiO_2, allowing the photogenerated electrons to react with more O_2 to form reactive substances, such as $\cdot O_2^-$, ·OH, etc., thereby further increasing the catalytic activity of the catalysts [27,28]; (3) or that Ag/TiO_2-5 W-50 s has a strong adsorption effect on organic compounds (e.g., MO) containing N and S functional groups, and in the oxygen-enriched state (O_2 adsorption from the crystal surface of anatase TiO_2(101)), the connection between MO and TiO_2 is in the form of S-O bonds [31].

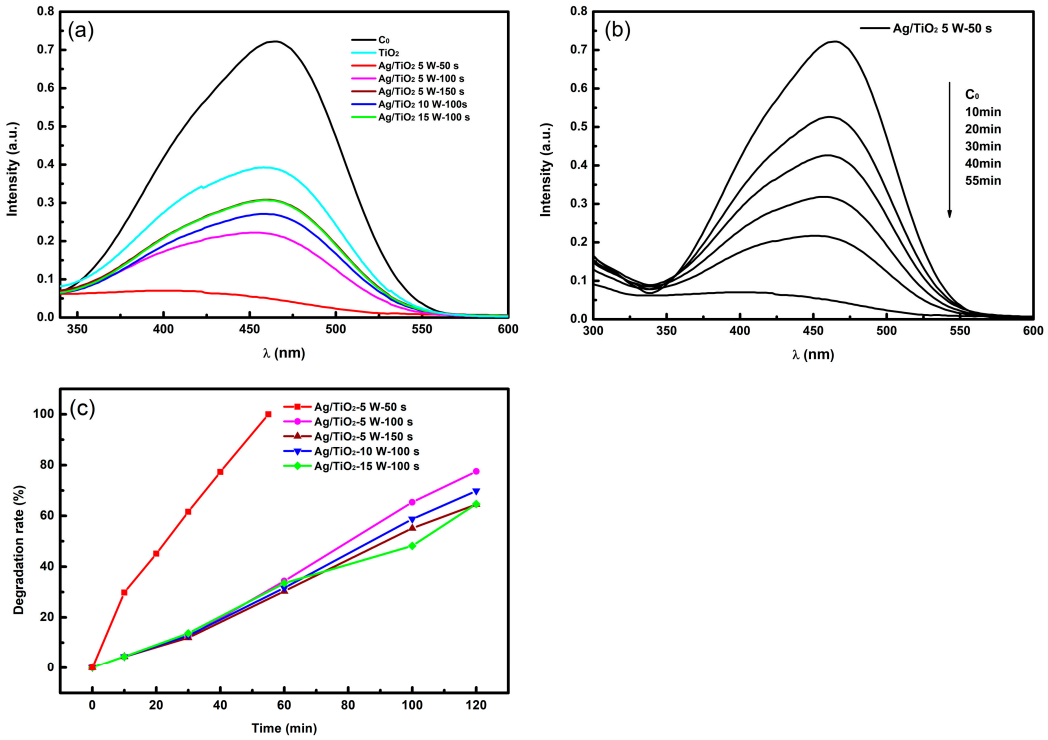

Figure 5. UV-Vis spectra of MO solution after the photocatalytic degradation reaction via (**a**) TiO_2 and Ag/TiO_2; (**b**) time-dependent UV-Vis spectra of MO degraded with Ag/TiO_2-5 W-50 s in pure MO solution during the photocatalytic degradation process; (**c**) degradation rate of MO degraded with Ag/TiO_2 in pure MO solution.

In keeping the experimental conditions unchanged, the recovered photocatalyst with the best degradation effect (Ag/TiO_2-5 W-50 s films) was used to degrade MO. Figure 6 shows the photocatalytic effect of the recycled photocatalyst. Figure 6a shows UV-Vis absorption spectra of MO solution after different cycles of photocatalytic degradation in pure MO solution. The degradation rate of MO (C_0 = 10 mg L^{-1}) using Ag/TiO_2-5 W-50 s with different cycles in pure MO solution is shown in Figure 6b. It can be found that the degradation effect of the first time is the best, reaching 100% in only 55 min, and the degradation rate of the fourth cycle is 100%, but this takes 90 min. Although the final degradation rate can reach 100%, the degradation time extends significantly as the number of cycles increases. This occurrence is caused by some water-insoluble or intermediate water-insoluble products that have been adsorbed on the catalyst's surface, which affects the adsorption performance and absorbance of the catalyst and reduces the degradation effect [24]. In addition, Ag particles can be oxidized, leading to an increase in the recombination rate of photogenerated electron–hole pairs, reducing the utilization rate of photogenerated charge carriers [32,33].

Figure 7a shows the time-dependent optical absorption spectra of MO with an initial MO concentration of 10 mg/L and Na_2SO_4 concentration of 12.5 g/L in the mixture solution of MO-Na_2SO_4 before and after photocatalytic degradation with Ag/TiO_2-5 W-50 s. It can be found that the degradation of pure MO in pure solution was completed in 55 min, and the degradation rate of MO can reach 100% while the degradation rate of MO in MO-Na_2SO_4 mixed solution can reach 100% in 65 min, as shown in Figure 7b. By comparison, it can be found that the degradation effect of MO in pure MO solution is better than that in MO-Na_2SO_4 mixed solution. The results suggest that Na_2SO_4 has an inhibitory effect on the degradation of MO. The possible reason may be one of the following: (1) When Na_2SO_4 is added to the MO solution, the pH value of the solution increases. The photocatalytic degradation efficiency of Ag/TiO_2 at low pH is higher than that at high pH due to the fact that MO is an anionic molecule and positively charged photocatalyst surfaces are

more likely to absorb dye molecules. The dye structure of MO was prone to oxidation over the azo structure as the sulfonic groups ($-SO_4^-$) can help capture hydrogen protons and further enhance the hydrophobicity of the TiO_2 surface [34,35]. (2) When Na_2SO_4 is added to the MO solution, the saturation adsorption amount may decrease due to the competition adsorption of anions added (SO_4^{2-}) and anion dye molecules onto the surface of TiO_2, which inactivates part of the catalyst and reduces the degradation efficiency [36–39]. (3) SO_4^{2-} is adsorbed on the surface of the photocatalyst, acting as a pore-trapping agent to increase the content of $SO_4^-\cdot$ generated, which accelerates the oxidation of Ag and increases the recombination rate of photogenerated electron–hole pairs. This speculation can be supported by the XPS results in the following text.

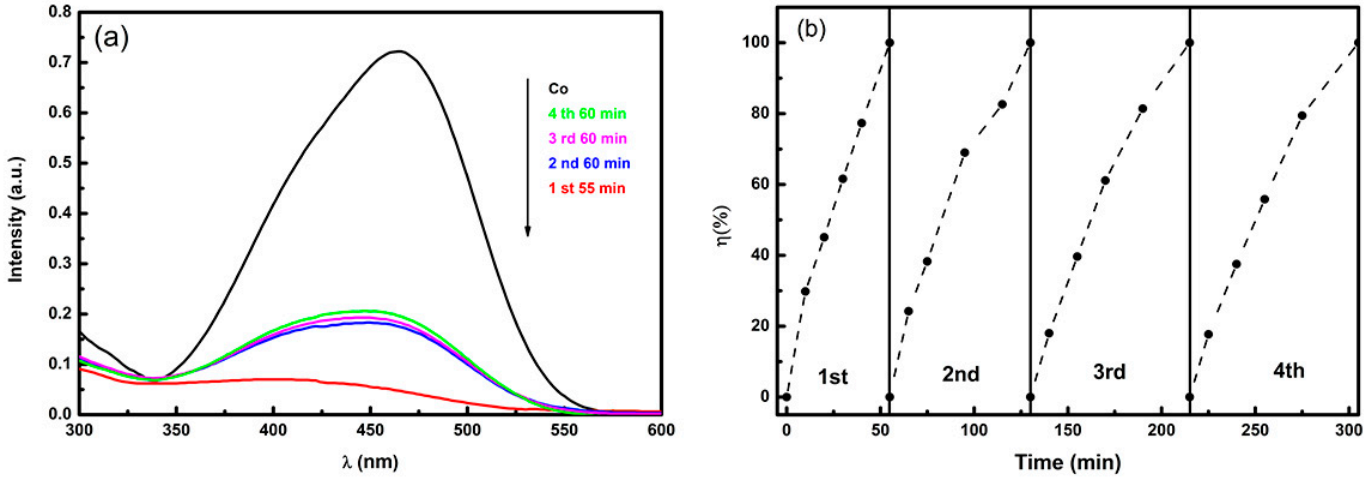

Figure 6. UV-Vis spectra of MO solution after the different cycles of photocatalytic degradation reaction in pure MO solution using (**a**) Ag/TiO_2-5 W-50 s; (**b**) the degradation rate of MO using Ag/TiO_2-5 W-50 s with different cycles.

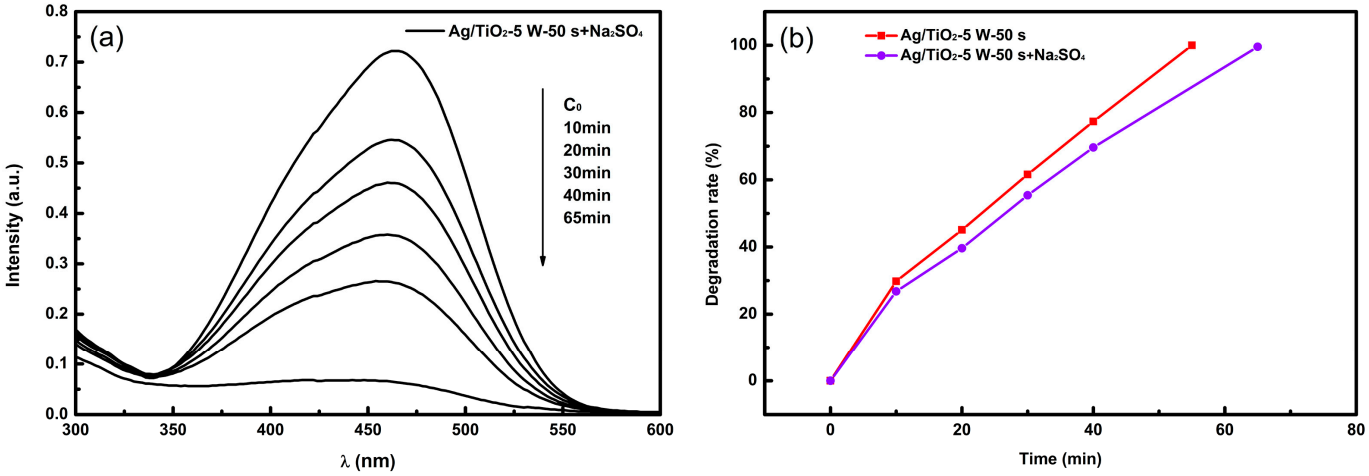

Figure 7. (**a**) Time-dependent UV-Vis spectra of MO degraded with Ag/TiO_2-5 W-50 s in MO-Na_2SO_4 mixed solution during the photocatalytic degradation process. (**b**) The degradation rates of MO in pure MO solution and MO-Na_2SO_4 mixed solution, respectively.

In order to study the elemental composition and chemical status of the Ag/TiO_2 before and after photocatalytic degradation, for the high-resolution XPS spectra of C, the peak at 284.80 eV appeared in all the samples, which can be assigned to the adventitious carbon. Figure 8 shows the XPS spectra of Ag/TiO_2-5 W-50 s before and after the photocatalytic degradation in different solutions. Figure 8a shows the wide-scan XPS spectra of the Ag/TiO_2-5 W-50 s before the photocatalytic degradation. According to the wide-scan XPS

spectra, Ti, Ag, O, and C are found as the surface elements of the prepared composites. Figure 8b shows the Ag $3d_{5/2}$ peak and Ag $3d_{3/2}$ peak of the Ag/TiO_2-5 W-50 s before the photocatalytic degradation. For Ag 3d corresponding to Ag^0, the binding energies for $3d_{5/2}$ and $3d_{3/2}$ electrons are observed around 367.7 eV and 373.7 eV, respectively [32]. The spin energy presents a characteristic value of 6.0 eV, which can be applied to confirm the presence of Ag^0 on the surface of Ag/TiO_2-5 W-50 s in Figure 8b. In addition, Ag/TiO_2-5 W-50 s also contained a small amount of silver oxide, and the binding energies of Ag_2O at approximately 367.2 and 373.2 eV can be assigned to $3d_{5/2}$ and $3d_{3/2}$, respectively [40–42] in Figure 8b, and the fitting results indicate that the proportion of Ag^+ in all Ag elements is 5.6%, which may be due to the surface oxidation of silver particles caused by exposure to air. Figure 8c shows the XPS spectrum of the Ti 2p of the Ag/TiO_2-5 W-50 s before the photocatalytic degradation. The spectrum of Ti $2p_{3/2}$ is symmetrical; that is to say, the spectrum of Ti $2p_{3/2}$ is consistent with single-state, the binding energy of the peak is 458.3 eV, and the distance between the peaks of Ti $2p_{1/2}$(464 eV) and Ti $2p_{3/2}$ is 5.7 eV. The results are the same as the data of a standard XPS of TiO_2 [43,44]. Consequently, it can be inferred that the titanium ions in Ag/TiO_2 are in the form of Ti^{4+}, while Ti^{3+} is not present in Ag/TiO_2.

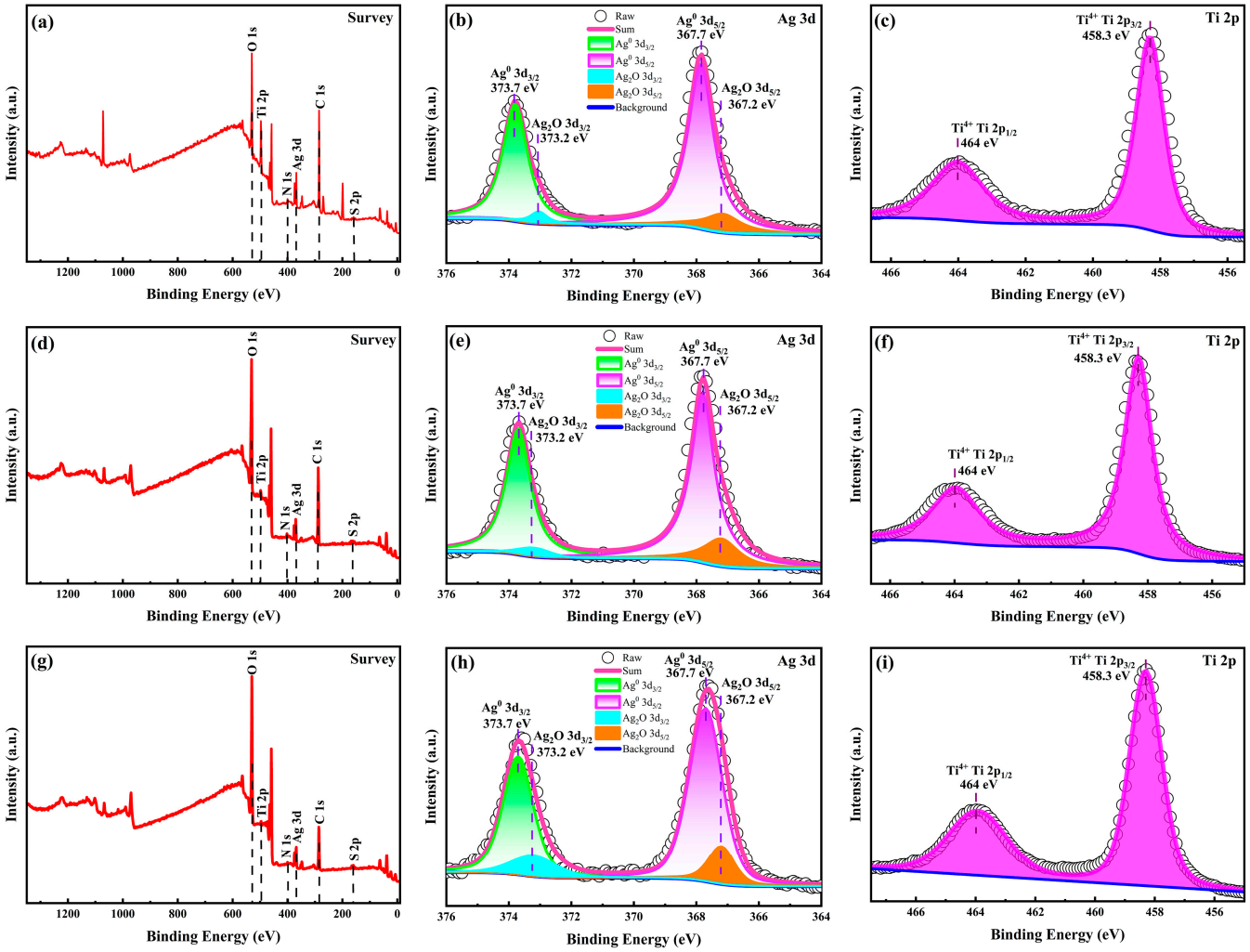

Figure 8. XPS spectra of Ag/TiO_2-5 W-50 s film before photocatalytic degradation of MO: (**a**) overall spectrum, (**b**) Ag 3d, and (**c**) Ti 2p; Ag/TiO_2-5 W-50 s film after the photocatalytic degradation of MO in pure MO solution: (**d**) overall spectrum, (**e**) Ag 3d, and (**f**) Ti 2p; Ag/TiO_2-5 W-50 s film after the photocatalytic degradation of MO in MO-Na_2SO_4 solution: (**g**) overall spectrum, (**h**) Ag 3d, and (**i**) Ti 2p.

Figure 8d–f show the wide-scan XPS spectra, Ag 3d, and Ti 2p of the Ag/TiO_2-5 W-50 s XPS spectra after photocatalytic degradation in pure MO solution, respectively. The characteristic peaks of C 1s, Ag 3d, N 1s, Ti 2p, O 1s, and S 2p were detected sequentially in the sample as shown in Figure 8d. Figure 8e shows the XPS spectrum of the amplified Ag 3d of Ag/TiO_2-5 W-50 s after photocatalytic degradation in pure MO solution. The Ag $3d_{5/2}$ peak at 367.7 eV and the Ag $3d_{3/2}$ peak at 373.7 eV correspond to Ag^0, and the Ag $3d_{5/2}$ peak at 367.2 eV and the Ag $3d_{3/2}$ peak at 373.2 eV correspond to Ag^+. The fitting results indicate that the proportion of Ag^+ in all Ag elements is 9.6%. It can be found that compared with the results in Figure 8b, the increase in Ag^+ is also one of the reasons for the decline in the degradation effect in the cyclic experiment. As the oxidation degree of silver is intensified, the plasma resonance effect is weakened, the ability of bound electrons is reduced, and the recombination rate of photogenerated electron–hole pairs is increased [29,30]. Figure 8f shows the XPS spectrum of the Ti 2p of the Ag/TiO_2-5 W-50 s after photocatalytic degradation in pure MO solution. The results are consistent with those in Figure 8c.

Figure 8g–i show the wide-scan XPS spectra, Ag 3d, and Ti 2p of the Ag/TiO_2-5 W-50 s XPS spectra after photocatalytic degradation in MO-Na_2SO_4 mixed solution, respectively. The characteristic peaks of C 1s, Ag 3d, N 1s, Ti 2p, O 1s, and S 2p were detected in the sample as shown in Figure 8g. Figure 8h shows the XPS spectrum of the amplified Ag 3d of Ag/TiO_2-5 W-50 s after photocatalytic degradation in the MO-Na_2SO_4 mixed solution. The Ag $3d_{5/2}$ peak at 367.7 eV and the Ag $3d_{3/2}$ peak at 373.7 eV correspond to Ag^0, and the Ag $3d_{5/2}$ peak at 367.2 eV and the Ag $3d_{3/2}$ peak at 373.2 eV correspond to Ag^+. The fitting results indicate that the proportion of Ag^+ in all Ag elements is 15.5%. It can be found that compared with the relative content of Ag^+ in Figure 8b,e, the increase in the proportion of Ag^+ is attributed to the fact that the Na_2SO_4 presence accelerates the oxidation of Ag^0 in the MO-Na_2SO_4 mixed solution, which is the reason for the decrease in photocatalytic degradation effect with the increase in degradation cycles. Figure 8f shows the XPS spectrum of the Ti 2p of the Ag/TiO_2-5 W-50 s after photocatalytic degradation in the MO-Na_2SO_4 mixed solution. The results are consistent with those in Figure 8c,f.

The reaction rate was calculated via linear fitting according to the first-order kinetics equation of degradation. The formula for the first-order kinetic equation for degradation is [45]

$$\ln\left(\frac{C_0}{C_t}\right) = kt \quad (3)$$

where t is the irradiation time, C_0 (mg L^{-1}) and C_t (mg L^{-1}) are the same as those in Equation (1), and k is the pseudo-first-order rate constant (min^{-1}). In the experiments, the photocatalytic degradation efficiency for MO was represented by the initial k. The initial k was obtained using experimental data up to 40 min of the simulated irradiation because the subsequent data seemed to deviate from the linear plot of ln (C_0/C_t) vs. t, owing to the decreasing MO concentration in the bulk solution. The linear regression coefficient R^2 of Ag/TiO_2-5 W-50 s and the initial rate constant k in the pure MO solution were 0.98634 and 0.04543 min^{-1}; meanwhile, in the MO-Na_2SO_4 solution, the linear regression coefficient R^2 was 0.98954 and the initial rate constant k was 0.03609 min^{-1}, as shown in Figure 9. Apparently, the linear regression coefficients of both were close to 1, which suggested that the pseudo-first-order kinetic was suitable for describing the kinetics of MO photodegradation; the photocatalytic process was a concentration-controlled reaction rate. And, the k value in the MO solution is larger than that in MO-Na_2SO_4, so the photocatalytic degradation efficiency of MO using Ag/TiO_2-5 W-50 s in the pure MO solution is better than that in the MO-Na_2SO_4 solution. The results are consistent with those in Figure 7b.

Figure 10 shows the schematic diagram of the photocatalytic degradation mechanism of Ag/TiO_2. Under UV irradiation, the photogenerated electrons in the TiO_2 conduction band migrate to Ag, forming electron–hole pairs. Consequently, a Schottky barrier is formed at the Ag-TiO_2 interface, acting as an electron trap. As a result, the electron capture sites on Ag inhibit the recombination of e^- and h^+, causing more residual h^+ in

the TiO_2 valence band to oxidize H_2O on the membrane surface, generating ·OH and increasing the ·OH concentration, thereby promoting the oxidative decomposition of MO. Simultaneously, the e^- captured on Ag can independently transfer to the adsorbed oxygen on the membrane surface, producing O_2^-, which also facilitates the degradation of MO [46]. While a large amount of SO_4^{2-} appeared in the solution after the addition of Na_2SO_4, SO_4^{2-} was adsorbed on the surface of the photocatalyst, acting as a pore-trapping agent to increase the generated content of SO_4^-·; both ·OH and SO_4^-· can make the Ag^0 on the surface of the catalyst oxidize to Ag^+, leading to the decrease in the degradation efficiency of the photocatalyst in the solution of MO-Na_2SO_4 [34].

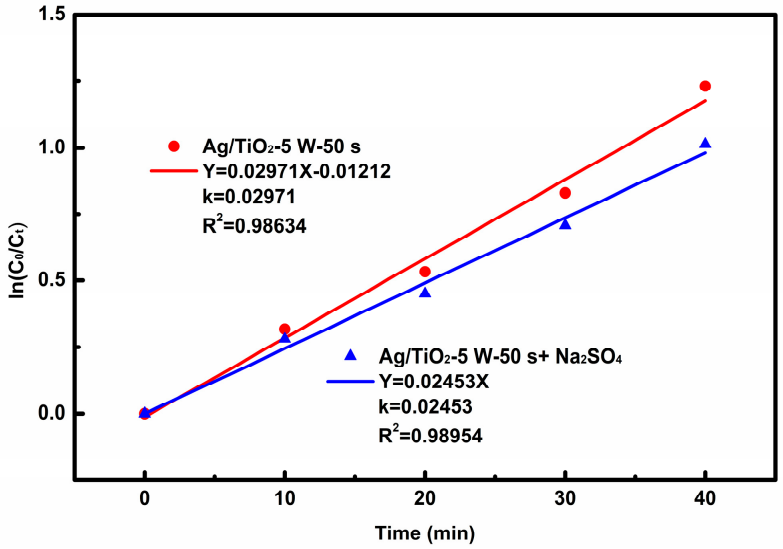

Figure 9. The first-order kinetic reactions for photocatalytic degradation of MO in pure MO solution and MO-Na_2SO_4 mixed solution through Ag/TiO_2-5 W-50 s.

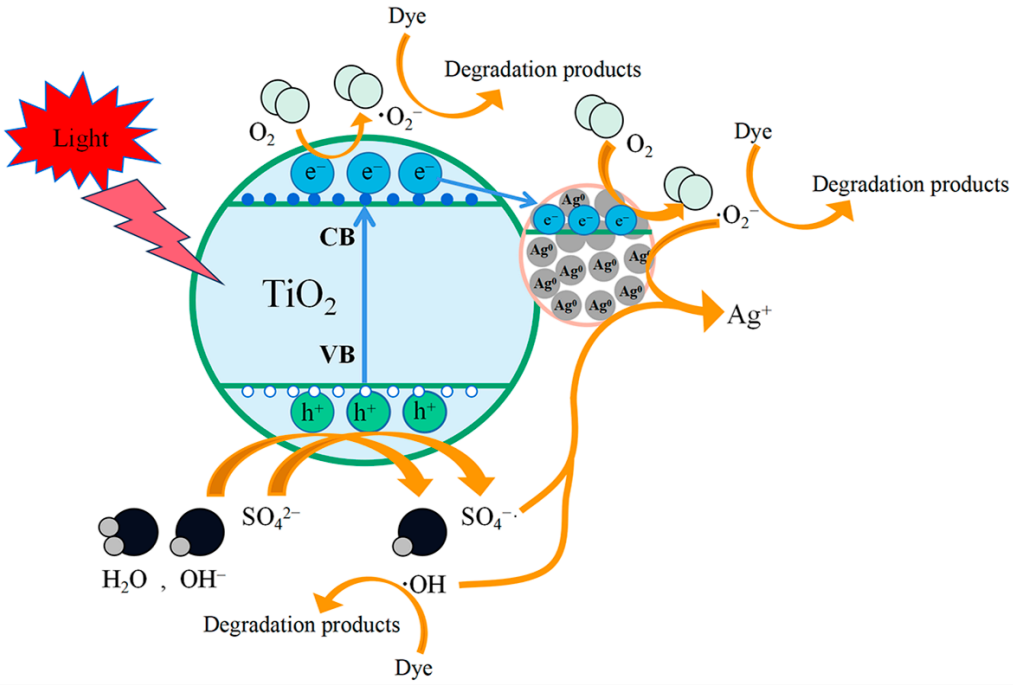

Figure 10. Schematic illustration of photocatalytic degradation mechanism of Ag/TiO_2 in MO-Na_2SO_4 mixed solution.

4. Conclusions

In this experiment, TiO_2 and Ag/TiO_2 films were prepared via DC magnetron sputtering, and the effect of silver modification on the photocatalytic performance was controlled using different sputtering power and sputtering times. The results show that the addition of Ag significantly enhances the visible light absorption of the catalyst, which is primarily because the addition of Ag prevents the recombination of photogenerated electrons and holes, effectively reduces the band gap of TiO_2, and forms the carrier trapping trap, which improves the photocatalytic redox ability of the film. The best photocatalytic degradation of Mo is through Ag/TiO_2-5 W-50 s, and the degradation rate can reach 100% within 55 min of light irradiation. After four test cycles, the degradation rate can still reach 100%, but more time is needed. However, the photocatalytic degradation efficiency of MO in MO-Na_2SO_4 solution can reach 99.55% within 65 min. The results indicate that the presence of Na_2SO_4 in MO solution can inhibit the degradation of MO through Ag/TiO_2. The principal cause of the degradation efficiency decreasing (MO) in the MO-Na_2SO_4 solution may be that the addition of Na_2SO_4 leads to the increase in pH, which is not conducive to the adsorption of dyes. SO_4^{2-} is adsorbed on the surface of the photocatalyst, acting as a pore-trapping agent to increase the content of $SO_4^{-}\cdot$generated, and the oxidation degree of Ag is intensified. In addition, the added anion (SO_4^{2-}) and anionic dye molecules competed for adsorption onto the Ag/TiO_2-5 W-50 s surface, thereby deactivating part of the catalyst and reducing the degradation efficiency.

Author Contributions: Conceptualization, L.S. and Z.Y.; methodology, L.S. and Z.Q.; software, T.R. and Z.Q.; validation, L.S., Z.Y. and Z.Q.; formal analysis, L.S., Z.Y. and Z.Q.; investigation, Z.Y. and Y.L.; resources, L.S. and Z.Y.; data curation, L.S. and Z.Q.; writing—original draft preparation, L.S. and Z.Y.; writing—review and editing, L.S. and Z.Y.; visualization, T.R. and Z.C.; supervision, L.S. and W.G.; project administration, L.S. and Z.Y.; funding acquisition, L.S. and S.M. All authors have read and agreed to the published version of the manuscript.

Funding: This research was funded by the National Natural Science Foundation of China, grant number 11904268, and the Hubei Province Education Department of China, grant number Q20181702.

Institutional Review Board Statement: Not applicable.

Informed Consent Statement: Not applicable.

Data Availability Statement: The original contributions presented in the study are included in the article, further inquiries can be directed to the corresponding author.

Conflicts of Interest: The authors declare no conflicts of interest.

References

1. Chen, P.; Ma, X.; Zhong, Z.; Zhang, F.; Fan, Y. Performance of ceramic nanofiltration membrane for desalination of dye solutions containing NaCl and Na_2SO_4. *Desalination* **2017**, *404*, 102–111. [CrossRef]
2. Huayna, G.; Laura, A.; Churata, R.; Lazo, L.; Guzmán, R.; Ramos, P.G.; Rodriguez, J.M. Synthesis and Characterization of a Photocatalytic Material from TiO_2 Nanoparticles Supported on Zeolite Obtained from Ignimbrite Residue Used in Decolorization of Methyl Orange. *Appl. Sci.* **2024**, *14*, 3146. [CrossRef]
3. Ioannidou, T.; Anagnostopoulou, M.; Papoulis, D.; Christoforidis, K.C.; Vasiliadou, I.A. UiO-66/Palygorskite/TiO_2 Ternary Composites as Adsorbents and Photocatalysts for Methyl Orange Removal. *Appl. Sci.* **2022**, *12*, 8223. [CrossRef]
4. Kuo, C.G.; Hsu, C.Y.; Wang, S.S.; Wen, D.C. Photocatalytic characteristics of TiO_2 films deposited by magnetron sputtering on polycarbonate at room temperature. *Appl. Surf. Sci.* **2012**, *258*, 6952–6957. [CrossRef]
5. Kavaliūnas, V.; Čeplikas, P.; Sriubas, M.; Laukaitis, G. The Sensitization of TiO_2 Thin Film by Ag Nanoparticles for the Improvement of Photocatalytic Efficiency. *Appl. Sci.* **2022**, *12*, 5725. [CrossRef]
6. Mekasuwandumrong, O.; Jantarasorn, N.; Panpranot, J.; Ratova, M.; Kelly, P.; Praserthdam, P. Synthesis of Cu/TiO_2 catalysts by reactive magnetron sputtering deposition and its application for photocatalytic reduction of CO_2 and H_2O to CH_4. *Ceram. Int.* **2019**, *45*, 22961–22971. [CrossRef]
7. Mourão, H.A.J.L.; Ribeiro, C. TiO_2 and SnO_2 magnetic nanocomposites: Influence of semiconductors and synthetic methods on photoactivity. *J. Nanosci. Nanotechnol.* **2011**, *11*, 7876–7883. [CrossRef] [PubMed]
8. Liu, G.; Wang, L.; Yang, H.G.; Cheng, H.M.; Lu, G.Q. Titania-based photocatalysts—Crystal growth, doping and heterostructuring. *J. Mater. Chem.* **2010**, *20*, 831–843. [CrossRef]

9. Zouheir, M.; Tanji, K.; Navio, J.A.; Hidalgo, M.C.; Jaramillo-Páez, C.A.; Kherbeche, A.D.H. Effective photocatalytic conversion of formic acid using iron, copper and sulphate doped TiO_2. *J. Cent. South Univ.* **2022**, *29*, 3592–3607. [CrossRef]
10. Wang, P.; Li, X.Y.; Shi, Z.L.; Li, H.T. Synergistic Effect of Ag and Ag_2O on Photocatalytic H_2-evolution Performance of TiO_2. *J. Inorg. Mater.* **2020**, *35*, 781–788.
11. Zhang, K.; Park, J.H. Surface Localization of Defects in Black TiO_2: Enhancing Photoactivity or Reactivity. *J. Phys. Chem. Lett.* **2017**, *8*, 199–207. [CrossRef] [PubMed]
12. Zuo, J. Deposition of Ag nanostructures on TiO_2 thin films by RF magnetron sputtering. *Appl. Surf. Sci.* **2010**, *256*, 7096–7101. [CrossRef]
13. Gao, Y.; Zhang, W.; Liu, P. Enhanced Photocatalytic Efficiency of TiO_2 Membrane Decorated with Ag and Au Nanoparticles. *Appl. Sci.* **2018**, *8*, 945. [CrossRef]
14. Pugazhenthiran, N.; Murugesan, S.; Anandan, S. High surface area Ag-TiO_2 nanotubes for solar/visible-light photocatalytic degradation of ceftiofur sodium. *J. Hazard. Mater.* **2013**, *263*, 541–549. [CrossRef] [PubMed]
15. Yang, J.; Luo, X. Ag-doped TiO_2 immobilized cellulose-derived carbon beads: One-Pot preparation, photocatalytic degradation performance and mechanism of ceftriaxone sodium. *Appl. Surf. Sci. J. Devoted Prop. Interfaces Relat. Synth. Behav. Mater.* **2021**, *542*, 148724. [CrossRef]
16. Kumaravel, V.; Mathew, S.; Bartlett, J.; Pillai, S.C. Photocatalytic hydrogen production using metal doped TiO_2: A review of recent advances. *Appl. Catal. B Environ.* **2018**, *244*, 1021–1064. [CrossRef]
17. Yuan, X.; Liang, S.; Ke, H.; Wei, Q.; Huang, Z.; Chen, D. Photocatalytic property of polyester fabrics coated with Ag/TiO_2 composite films by magnetron sputtering. *Vacuum* **2020**, *172*, 109103. [CrossRef]
18. Ichimura, A.S.; Mack, B.M.; Usmani, S.M.; Mars, D.G. Direct Synthesis of Anatase Films with 100% (001) Facets and [001] Preferred Orientation. *Chem. Mater.* **2012**, *24*, 2324–2329. [CrossRef]
19. Zhang, Y.J.; Zhao, D.F.; Cao, C.; Hou, H.F.; Yu, Q.Z. Research Advancement and Tendency of Nano TiO_2 Photocatalytic Treatment of Waste Water. *J. Jiaxing Univ.* **2010**, *6*, 67–72.
20. Kisch, H.; Sakthivel, S.; Janczarek, M.; Mitoraj, D. A Low-Band Gap, Nitrogen-Modified Titania Visible-Light Photocatalyst. *J. Phys. Chem. C* **2007**, *111*, 11445–11449. [CrossRef]
21. Li, W.; Wang, F.; Liu, Y.; Wang, J.; Yang, J.; Zhang, L.; Elzatahry, A.A.; Al-Dahyan, D.; Xia, Y.; Zhao, D. General strategy to synthesize uniform mesoporous TiO_2/graphene/mesoporous TiO_2 sandwich-like nanosheets for highly reversible lithium storage. *Nano Lett.* **2015**, *15*, 2186. [CrossRef] [PubMed]
22. Nie, L.; Yu, J.; Li, X.; Cheng, B.; Liu, G.; Jaroniec, M. Enhanced performance of NaOH-modified Pt/TiO_2 toward room temperature selective oxidation of formaldehyde. *Environ. Sci. Technol.* **2013**, *47*, 2777–2783. [CrossRef] [PubMed]
23. Bastow, T.J.; Whitfield, H.J. 47,49Ti NMR: Evolution of Crystalline TiO_2 from the Gel State. *Chem. Mater.* **1999**, *11*, 3518–3520. [CrossRef]
24. Sun, L.; Zhou, Q.; Mao, J.; Ouyang, X.; Yuan, Z.; Song, X.; Gong, W.; Mei, S.; Xu, W. Study on Photocatalytic Degradation of Acid Red 73 by Fe_3O_4@TiO_2 Exposed (001) Facets. *Appl. Sci.* **2022**, *12*, 3574. [CrossRef]
25. Kim, Y.; Kim, J.; Chang, M.; Park, B. Carrier depletion mediated exciton-surface plasmon coupling at the mesoporous TiO_2/Ag interface. *Appl. Surf. Sci.* **2022**, *575*, 151690. [CrossRef]
26. Zang, L.; Liu, C.Y.; Ren, X.M. Photochemistry of semiconductor particles. Part 4.—Effects of surface condition on the photodegradation of 2,4-dichlorophenol catalysed by TiO2 suspensions. *J. Chem. Soc. Faraday Trans.* **2015**, *91*, 917–923. [CrossRef]
27. Guo, J.; Watanabe, S.; Janik, M.J.; Ma, X.; Song, C. Density functional theory study on adsorption of thiophene on TiO_2 anatase (001) surfaces. *Catal. Today* **2010**, *149*, 218–223. [CrossRef]
28. Li, X.Z.; Li, F.B. Study of Au/Au($^{3+}$)-TiO_2 photocatalysts toward visible photooxidation for water and wastewater treatment. *Environ. Sci. Technol.* **2001**, *35*, 2381–2387. [CrossRef]
29. Linsebigler, A.; Lu, G.; Yates, J. Photocatalysis on TiO_2 Surfaces: Principles, Mechanisms, and Selected Results. *Chem. Rev.* **1995**, *95*, 735–758. [CrossRef]
30. You, X.; Chen, F.; Zhang, J.; Anpo, M. A novel deposition precipitation method for preparation of Ag-loaded titanium dioxide. *Catal. Lett.* **2005**, *102*, 247–250. [CrossRef]
31. Hussain, A.S.; McKee, M.L.; Heinzel, J.M.; Sun, X.; Tatarchuk, B.J. Density Functional Theory Study of Organosulfur Selective Adsorption on Ag–TiO_2 Adsorbents. *J. Phys. Chem. C* **2014**, *118*, 14938–14947. [CrossRef]
32. Chi, Y.; Yuan, Q.; Li, Y.; Zhao, L.; Yan, W. Magnetically separable Fe_3O_4@SiO_2@TiO_2-Ag microspheres with well-designed nanostructure and enhanced photocatalytic activity. *J. Hazard. Mater.* **2013**, *262C*, 404–411. [CrossRef]
33. Shaviv, E.; Schubert, O.; Alvessantos, M.; Goldoni, G.; Felice, R.D.; Fatti, N.D.; Banin, U. Absorption Properties of Metal-semiconductor Hybrid Nanoparticles. *ACS Nano* **2011**, *5*, 4712–4719. [CrossRef] [PubMed]
34. Al-Rasheed, R.; Cardin, D.J. Photocatalytic degradation of humic acid in saline waters. Part 1. Artificial seawater: Influence of TiO_2, temperature, PH, and air-flow. *Chemosphere* **2003**, *51*, 925–933. [CrossRef] [PubMed]
35. Geng, Q.; Cui, W. Adsorption and Photocatalytic Degradation of Reactive Brilliant Red K-2BP by TiO_2/AC in Bubbling Fluidized Bed Photocatalytic Reactor. *Ind. Eng. Chem. Res.* **2010**, *49*, 11321–11330. [CrossRef]
36. Bhatkhande, D.S.; Kamble, S.P.; Sawant, S.B.; Pangarkar, V.G. Photocatalytic and photochemical degradation of nitrobenzene using artificial ultraviolet light. *Chem. Eng. J.* **2004**, *102*, 283–290. [CrossRef]

37. Bhatkhande, D.S.; Pangarkar, V.G.; Beenackers, A.A.C.M. Photocatalytic degradation of nitrobenzene using titanium dioxide and concentrated solar radiation: Chemical effects and scaleup. *Water Res.* **2003**, *37*, 1223–1230. [CrossRef] [PubMed]
38. Bhatkhande, D.S.; Sawant, S.B.; Schouten, J.C.; Pangarkar, V.G. Photocatalytic degradation of chlorobenzene using solar and artificial UV radiation. *J. Chem. Technol. Biotechnol.* **2004**, *79*, 354–360. [CrossRef]
39. Lv, K.; Xu, Y. Effects of polyoxometalate and fluoride on adsorption and photocatalytic degradation of organic dye X3B on TiO_2: The difference in the production of reactive species. *J. Phys. Chem. B* **2006**, *110*, 6204–6212. [CrossRef]
40. Chen, Y.; Huang, W.; He, D.; Situ, Y.; Huang, H. Construction of Heterostructured g-C_3N_4/Ag/TiO_2 Microspheres with Enhanced Photocatalysis Performance under Visible-Light Irradiation. *ACS Appl. Mater. Interfaces* **2014**, *6*, 14405–14414. [CrossRef]
41. Narkbuakaew, T.; Saito, N.; Sattayaporn, S.; Sujaridworakun, P. Investigation of the Ag species and synergy of Ag-TiO_2 and g-C_3N_4 for the enhancement of photocatalytic activity under UV-Visible light irradiation. *Appl. Surf. Sci. J. Devoted Prop. Interfaces Relat. Synth. Behav. Mater.* **2022**, *573*, 151617. [CrossRef]
42. Xin, B.; Jing, L.; Ren, Z.; Wang, B.; Fu, H. Effects of simultaneously doped and deposited Ag on the photocatalytic activity and surface states of TiO_2. *J. Phys. Chem. B* **2005**, *109*, 2805–2809. [CrossRef]
43. Briggs, D. Handbook of X-ray Photoelectron Spectroscopy C. D. Wanger, W.M. Riggs, L.E. Davis, J.F. Moulder and G. E.Muilenberg Perkin-Elmer Corp., Physical Electronics Division, Eden Prairie, Minnesota, USA, 1979. 190 pp. $195. *Surf. Interface Anal.* **1981**, *3*, v–v. [CrossRef]
44. Huang, D.; Liao, S.; Quan, S.; Liu, L.; He, Z.; Wan, J.; Zhou, W. Synthesis and characterization of visible light responsive N–TiO 2 mixed crystal by a modified hydrothermal process. *J. Non-Cryst. Solids* **2008**, *354*, 3965–3972. [CrossRef]
45. Ma, L.; Wang, G.; Jiang, C.; Bao, H.; Xu, Q. Synthesis of core-shell TiO2@g-C3N4 hollow microspheres for efficient photocatalytic degradation of rhodamine B under visible light. *Appl. Surf. Sci. J. Devoted Prop. Interfaces Relat. Synth. Behav. Mater.* **2018**, *430*, 263–272.
46. Zhiming, Z.; Jian, S.; Shaomin, X.; Dongjie, L.; Bailing, J. Enhanced Raman scattering and photocatalytic activity of TiO_2 films with embedded Ag nanoparticles deposited by magnetron sputtering. *J. Alloys Compd.* **2016**, *679*, 88–93.